NANO LETTERS

2008
Vol. 8, No. 1
340−344

Crossover from Kondo-Assisted Suppression to Co-Tunneling Enhancement of Tunneling Magnetoresistance via Ferromagnetic Nanodots in MgO Tunnel Barriers

Hyunsoo Yang, See-Hun Yang, and Stuart S. P. Parkin*

IBM Almaden Research Center, 650 Harry Road, San Jose, California 95120

Received November 9, 2007

ABSTRACT

The dependence of the tunneling magnetoresistance (TMR) of planar magnetic tunnel junctions on the size of magnetic nanodots incorporated within MgO tunnel barriers is explored. At low temperatures, in the Coulomb blockade (CB) regime, for smaller nanodots the conductance of the junction is increased at low bias consistent with Kondo-assisted tunneling and the TMR is suppressed. For slightly larger nanodots but within the CB regime, the TMR is enhanced at low bias, consistent with co-tunneling. Magnetic tunnel junctions (MTJ) exhibit giant magnetoresistance in small magnetic fields that arises from the flow of spin-polarized current through an ultrathin tunnel barrier separating two magnetic electrodes. The current through an MTJ device depends on the magnetic orientation of the electrodes and is typically higher when the electrode moments are parallel than when they are antiparallel.[1] It has recently been demonstrated that the spin polarization of the tunneling current can be greatly enhanced by using crystalline tunnel barriers formed from MgO as compared with conventional amorphous barriers formed from alumina, due to spin filtering across the MgO layer.[2−6] The magneto-transport properties of magnetic granular alloys and magnetic tunnel junction devices with magnetic nanodots embedded in amorphous dielectric matrices[7,8] and tunnel barriers,[9,10] respectively, have been studied by several groups, but no systematic studies of the dependence on these properties on the nanodot size have been made.

Here we show that a wide range of magneto-transport properties in magnetic tunnel junctions with barriers containing magnetic nanodots can be accounted for by Kondo-like physics and that as the size of these nanodots is systematically increased the tunneling properties change from those characteristic of Kondo tunneling, which suppresses the tunneling magnetoresistance (TMR) near zero bias, to those of correlated tunneling which increases the TMR at low bias.

The magnetic tunnel junction (MTJ) device (see Figure 1a) is composed of CoFe ferromagnetic (F) electrodes, and an MgO tunnel barrier.[2] Both F electrodes are exchange biased, but the exchange bias field is designed to be significantly stronger for the lower electrode so that the moment of each electrode can be switched independently. A thin CoFe layer of nominal thickness t_{ND} is inserted in the middle of the MgO layer. When this layer is thinner than ∼2 nm, it forms a discontinuous layer of nanodots, as revealed by plan-view transmission electron microscopy (TEM). This means that the diameter of the nanodots is considerably larger than the nominal layer thickness. For example, when t_{ND}= 0.25 and 0.75 nm, the nanodot diameters are estimated to be ∼1.53 ± 0.4and ∼3.2 ± 0.7 nm, respectively (see Figure 1b,c and Supporting Information). The chemical state of individual nanodots was examined by electron energy loss spectroscopy in a high-resolution scanning TEM, which revealed clear evidence for the presence of both metallic Co and Fe.

The magneto-transport properties of the MTJs are considerably affected by the presence of the nanodots in the MgO tunnel barrier, as shown in Figure 2. In particular, as the temperature is reduced the resistance of the MTJ increases, but at a greater rate the smaller the nanodot size is. This is due to a Coulomb blockade (CB) effect,[11] which has previously been seen in MTJs formed with discontinuous Co and Fe layers within alumina[10,12−14] and MgO[15] tunnel barriers. At high temperatures and bias voltages, the tunneling is dominated by sequential tunneling through the nanodots because the barrier is very thick (thus direct tunneling across the MgO barrier is small). The nanodots are so small that there is a significant increase in energy when an electron tunnels onto a dot which, at low temperature and bias compared to this energy, thereby depresses the tunneling conductance across the MTJ device.[9] By taking into account,

* To whom correspondence should be addressed. E-mail: parkin@almaden.ibm.com. Phone: (408) 927-2390.

10.1021/nl072930n CCC: $40.75
Published on Web 12/21/2007

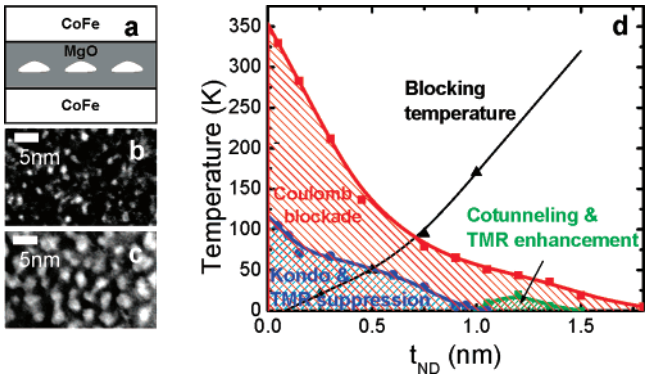

Figure 1. (a) Illustration of a magnetic tunnel junction device with a discontinuous layer deposited in the middle of the tunnel barrier, forming a layer of nanodots. (b,c) Plan view TEMs for $t_{ND} = 0.25$ nm and $t_{ND} = 0.75$ nm in related structures in which the top electrode is not grown but is substituted by 2 nm Mg and the bottom electrode is milled away to leave only the layer of CoFe nanodots sandwiched between MgO. White regions correspond to nanodots while black regions indicate MgO. (d) Phase diagram showing the dependence of the blocking temperature T_B, the Kondo temperature T_K, and the CB temperature on t_{ND}. The CB region is shaded in red. Within the blue region, the TMR is suppressed and the conductivity enhanced near zero bias, consistent with Kondo-assisted tunneling. By contrast, within the smaller green region the TMR is enhanced and the conductivity reduced near zero bias, consistent with co-tunneling. Solid lines through the data points are guides to the eye. Note that T_B corresponds to the blocking temperature of the largest nanodots (see the Supporting Information) so that smaller nanodots will have lower blocking temperatures.

both indirect and direct tunneling mechanisms (following ref 16, as discussed in detail in Supporting Information), the temperature dependence of the tunneling resistance can be well accounted for, as shown by the solid curves in Figure 3a. From these fits, a characteristic temperature T_{CB}, below which CB effects are important, can be derived. T_{CB} is proportional to the charging energy needed to add a single electron to the dot (see Supporting Information). CB effects are observed when $t_{ND} < 1.8$ nm with T_{CB} increasing to ~330 K when $t_{ND} = 0.05$ nm (see Figure 1d). The calculated CB energy is consistent with the average size of the nanodots inferred from plan-view TEM micrographs. For example, when $t_{ND} = 0.45$ nm, the CB energy is ~53 meV, which gives a nanodot diameter of ~2.6 nm (see Supporting Information).

The nanodots are so small that they are superparamagnetic,[17] which means that the direction of the magnetic moment of an individual nanodot fluctuates due to thermal fluctuations above a characteristic blocking temperature T_B. By contrast with the CB effect, T_B decreases as the nanodot volume is decreased. T_B was measured from the magnetic properties of multilayers of the form [3 nm MgO/t_{ND} CoFe]$_{20}$ because the magnetic signal from a single nanodot layer is too weak to be measured alone by SQUID magnetometry (Supporting Information, Figure S2). T_B was determined from the temperature at which the zero field-cooled (ZFC) magnetization shows a maximum value.[18] The dependence of T_B on t_{ND} is shown in Figure 1d. T_B is reduced below the CB temperature when t_{ND} is smaller than ~0.7 nm. The ZFC magnetization data show clear evidence for blocking effects with the magnetization dropping below T_B to nearly zero at 5 K. However, field-cooled (FC) data show evidence for a considerable dispersion in the size of the nanodots so that many nanodots remain unblocked with fluctuating magnetic moments even for temperatures well below T_B. Interestingly, as t_{ND} is increased the FC data show that an increasing proportion of the nanodot moments are blocked so that above $t_{ND} \sim 1$ nm most nanodot moments are blocked below T_B (see Supporting Information, Figure S2).

A second consequence of the CB phenomenon arising from the nanodots is a strongly enhanced bias voltage dependence of the tunneling resistance in the CB regime (that is, when $T < T_{CB}$) when the bias voltage is below the CB-charging energy.[14] The bias voltage dependence of the resistance of an MTJ with no nanodot layer and nanodot layers 0.45 nm and 1.2 nm thick are compared in Figure 2 for temperatures ranging from 2.5 to 300 K. The resistance of the pristine MTJ with its moments either parallel R_P or antiparallel R_{AP} shows a weak dependence on the bias voltage V (Figure 2a) for all temperatures. By contrast, at low temperatures R_P and R_{AP} decrease rapidly with V when the nanodot layer is present; the more rapidly the bigger the nanodot is. For the examples shown in Figure 2, at 2.5 K the resistance is decreased by half at $V \sim 26$ and 7 mV, when $t_{ND} = 0.45$ and 1.2 nm, respectively, for both the P and AP states. These voltages scale with T_{CB} (see Figure 1d) and are clearly related to the CB effect.

An important result is a strong suppression of the TMR at low temperatures and bias voltages in the CB regime when the nanodot layer is thinner than ~1 nm (Figure 2e,f). A similar phenomenon is observed for nanodot layers even as thin as 0.05 nm (see Figure 4). However, there is a small region of nanodot layer thickness when t_{ND} is slightly thicker than ~1 nm but still within the CB regime where we observe an enhancement of the TMR at low-bias voltage and temperature (see Figures 1d and 2i). This latter phenomenon has recently been observed in large-area MTJs with alumina tunnel barriers in which a nanodot layer formed from 1 nm thick $Co_{90}Fe_{10}$ was inserted[10] and was attributed to co-tunneling.[9] Co-tunneling is the correlated tunneling of electrons when sequential uncorrelated tunneling through the magnetic nanodots is suppressed for voltages below the CB charging energy E_{CB}.[9] Our observation of suppressed TMR for smaller nanodots was not predicted by this theory however, which did not consider spin-flip processes on the nanodots.

The suppression of TMR is consistent with theoretical models in which the spin-dependent tunneling through nominally nonmagnetic nanodots in the CB regime between ferromagnetic electrodes is considered.[19,20] In these models, the nanodots are so small that they contain a finite number of electrons, and thus in the CB regime when there are an odd number of electrons on the nanodot, the dot has a finite spin. The screening of the nanodot spin through a Kondo interaction with the spin-polarized electrons in the ferromagnetic electrodes was predicted to lead to a suppression of the TMR when $eV < E_{CB}$.[21] This effect has been observed in a very small number of samples in experiments in which

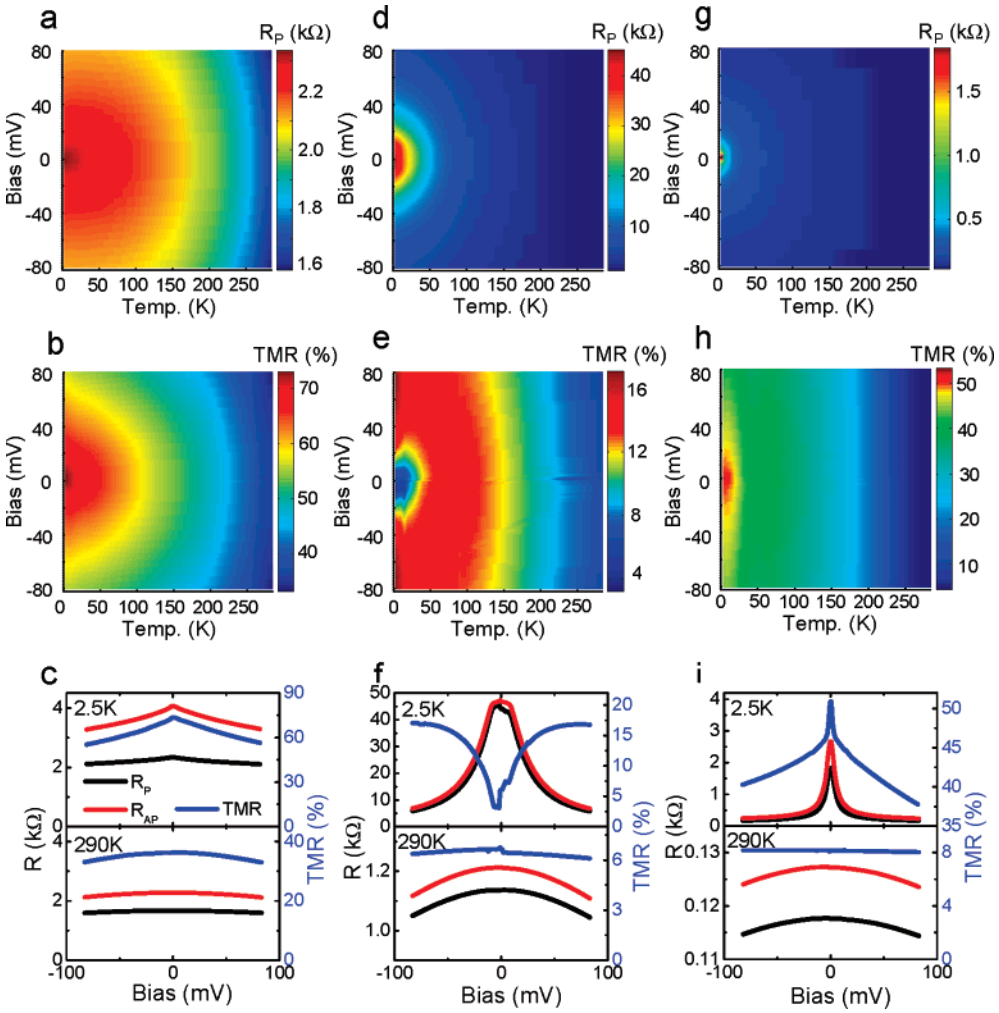

Figure 2. The temperature and bias voltage dependence of the dc resistance and TMR of a MTJ without the nanodot layer (a−c) and with a nanodot layer in (d−i). Data are shown for the resistance when the magnetic moments of the upper and lower exchange-biased ferromagnetic electrodes are parallel (P) and antiparallel (AP). The nanodot layer thickness is 0.45 nm in (d−f) and 1.2 nm in (g−i).

tunneling via individual (or possibly several) nonmagnetic C_{60} molecules between Ni electrodes was studied in break junctions formed by electromigration of a Ni point contact.[22] Here, we appear to observe a similar effect in planar macroscopic tunnel junctions in which tunneling takes place through many magnetic nanodots of a considerable size. For example, when $t_{ND} = 0.45$ nm we estimate that the nanodot contains ~600 atoms. Moreover, the CoFe nanodots have large magnetic moments: each atom has a moment at 2.5 K of ~1.8 μ_B. Kondo effects are usually considered to be important only when the magnetic moment being screened is small,[23] although recent theoretical work has suggested that Kondo effects may be possible with large magnetic moments when the magnetic moments have considerable magnetic anisotropy.[24,25] In our case, the magnetic nanodots are pancake-shaped (see Supporting Information), which will lead to significant magnetic anisotropy.

There are several other characteristic features of Kondo-assisted tunneling, which we observe in MTJs with nanodots. One of these is a peak in the tunneling conductance versus bias voltage curve centered at zero voltage that has a characteristic width proportional to the strength of the Kondo interaction, that is, the Kondo temperature T_K. The peak can be accounted for by a Kondo resonant-tunneling channel. Conductance versus voltage curves are compared in Figure 3b for MTJs with $t_{ND} = 0$ and 0.5 nm. The MTJ without nanodots shows a dip in conductance near zero bias, whereas MTJs with nanodot layers for thicknesses ranging from 0.05−1 nm show a conductance peak. From the half-width at half-maximum ΔV of the conductance peak, we can estimate $T_K \sim 55$ K from the relationship $\Delta V = k_B T_K/e$[26,27] with $t_{ND} = 0.5$ nm. We estimated T_K using two other methods. First, we considered the temperature dependence of the zero bias conductance peak. Because there is a considerable background to the conductance versus voltage curve due predominantly to the increasing number of available states in the receiving F electrode at higher bias voltages, we fitted the conductance curves at each temperature for voltages from ~2 ΔV to 50 mV with a second-order polynomial and subtracted this curve from the measured curve to calculate the enhanced conductance at zero bias $\Delta G_K/G_B$ relative to the fitted background conductance at zero bias G_B.[28] The temperature dependence of $\Delta G_K/G_B$, which is shown in Figure 3c for $t_{ND} = 0.2$ and 0.5 nm, can be well described by an empirical formula developed to account for the temperature dependence of the Kondo

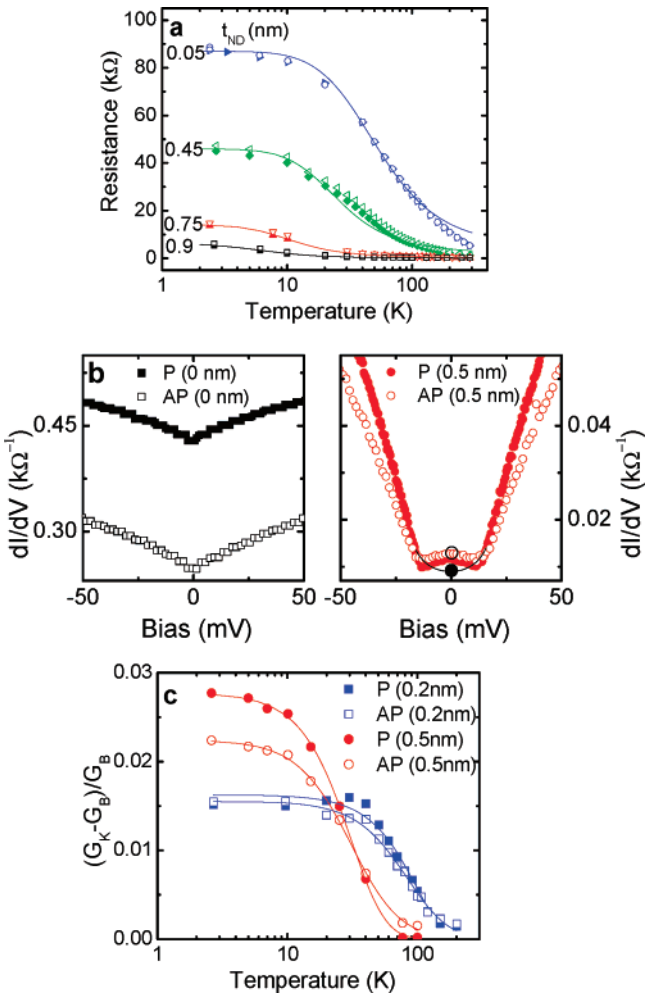

Figure 3. (a) The temperature dependence of the dc MTJ resistance at zero bias interpolated from current vs bias voltage curves. Examples are shown for four nanodot layer thicknesses indicated in the Figure. Filled (open) symbols correspond to R_P (R_{AP}) and solid lines are fits to the R_P data, as discussed in Supporting Information. (b) Differential conductance vs bias voltage curves at 2.5 K for the P and AP magnetic configurations for an MTJ without a nanodot layer (solid and open black squares) and an MTJ with a nanodot layer of thickness 0.5 nm (solid and open red circles). G_K (open black dot) is the measured conductance at zero bias, and G_B (solid black dot) is the conductance at zero bias interpolated by fitting the curves at higher voltages. (c) Temperature dependence of the conductance enhancement ratio $(G_K - G_B)/G_B$ for MTJs with $t_{ND} = 0.2$ and 0.5 nm in the P and AP configurations. The solid lines through the data are fits using the formula[29] $\Delta G_K(T)/G_B = G_0/1(1+(2^{1/s} - 1)T^2/ T_K^2)^s$ where $T_K = 31$ K ($s = 1.58$) and $T_K = 36$ K ($s = 0.98$) for the P and AP states, respectively, for the case of $t_{ND} = 0.5$ nm. For $t_{ND} = 0.2$ nm, $T_K = 76$ K ($s = 2.19$) and $T_K = 81$ K ($s = 1$) for the P and AP states, respectively.

conductance in a single electron transistor[29] and that has been widely used to describe the behavior in a variety of Kondo systems.[30,31] For the case of $t_{ND} = 0.2$ nm and for the P configuration, T_K, which we extract from this fit, is ~76 K, which compares well with the Kondo temperature derived from the conductance peak width at 2.5 K of ~ 69 K. Finally, the Kondo temperature can also be estimated, although more approximately, from the temperature at which the TMR is no longer suppressed at low-bias voltage. For example, from the detailed dependence of TMR on voltage and temperature

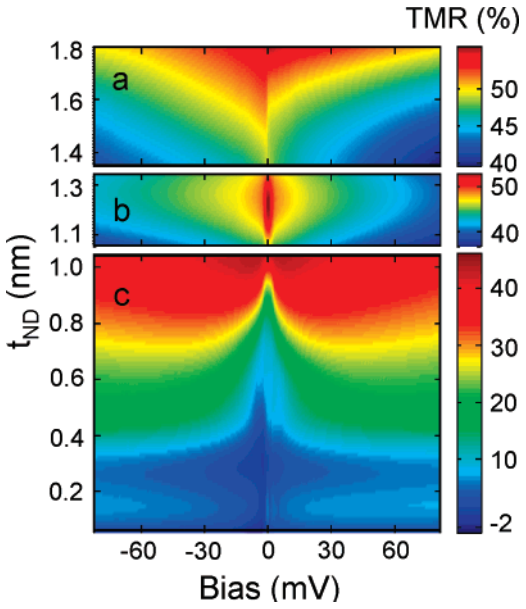

Figure 4. The bias voltage dependence of dc TMR at 2.5 K as a function of the nanodot layer thickness. The contour plots are created by interpolation between the experimental data points. To enhance the visibility of the TMR peaks (b) and dips (c) the plot is divided into 3 parts: (a) sequential tunneling ($t_{ND} = 1.35-1.8$ nm), (b) co-tunneling ($t_{ND} = 1-1.35$ nm), and (c) Kondo-assisted tunneling ($t_{ND} = 0.05-1$ nm) regimes. The color represents different TMR scales in each part.

for the case of $t_{ND} \sim 0.45$ nm shown in Figure 2e we estimate $T_K \sim 60$ K. We note that values of T_K are systematically higher by about 10−20% for the AP configuration.

The dependence of the Kondo temperature, derived from averaging the values found from the three methods discussed above, is plotted as a function of the nanodot layer thickness in Figure 1d. For the thinnest nanodot layer, $T_K \sim 100$ K, which is a very high Kondo temperature, but T_K decreases with increasing thickness to zero when t_{ND} is ~ 1 nm thick. From Figure 1d, it is clear that T_K is always significantly lower than T_{CB}, consistent with theoretical expectations that Kondo-assisted tunneling will only be found within the CB regime.[21] The high Kondo temperature might be indicative of a strong interaction between the ferromagnetic electrodes and the nanodots through the highly oriented MgO(100) tunnel barriers. Indeed, evidence for significant antiferromagnetic coupling of magnetic electrodes through MgO(100) barriers has been found.[32,33]

We note that the peak conductance near zero bias in the Kondo regime is several orders of magnitude below that calculated within the unitary limit. There are many possible reasons to account for this observation including the lack of tunability of the energy of the quantized electronic levels on the nanodots,[34] which will be very sensitive to the nanodot size and shape[35] and their magnetic configuration, interference within multiple conductance channels through individual nanodots, and asymmetry in the tunneling barriers.[36]

The detailed dependence of the voltage dependence of the tunneling magnetoresistance is plotted in Figure 4 as a function of the nanodot layer thickness at 2.5 K. We attribute the overall suppression of the maximum TMR observed as

t_{ND} is decreased to the reduced blocking temperature and the larger magnetic anisotropy of the smaller nanodots. This means that increasingly large magnetic fields are required to fully align the magnetic moments of the nanodots parallel to each other when the MTJ device is cooled. Because each device was cooled in a fixed field of 1 T, the degree of magnetic alignment is progressively reduced as t_{ND} is decreased and the nanodots become smaller. The data in Figure 4c show that as t_{ND} is increased from 0.05 to ~1 nm, the relative reduction of TMR at zero bias from its maximum value at each t_{ND} becomes increasingly smaller (see Supporting Information, Figure S4). The suppression of TMR is such that in many cases, and always for the very smallest nanodots, the TMR becomes negative, that is, the conductance becomes greater for the AP alignment of the ferromagnetic electrodes than for the P alignment (see Figure 3b). This inversion of the sign of the TMR is attributed to an exchange of the electron's spin as it tunnels via a virtual state on the nanodot. This is consistent with a Kondo phenomenon.[23,34] The enhancement of TMR at low bias seen for nanodot layers with thicknesses in the narrow range of ~1−1.4 nm can also be clearly seen in Figure 4b (see also Figure 2h). Outside the CB regime, the TMR has a weak dependence on voltage (below ±100 mV, the range shown in Figure 4a).

It is interesting to note that the crossover from a Kondo-like tunneling phenomenon with enhanced conductance and suppressed TMR to a regime of depressed conductance and enhanced TMR at low bias occurs at a nanodot layer thickness of ~1 nm. This is the same thickness below which field-cooled magnetization data indicates a dispersion of nanodot-blocking temperatures and considerable fluctuations of nanodot magnetic moments persisting to low temperatures and above which there is a single nanodot-blocking temperature. Thus, the crossover from Kondo to co-tunneling behavior is likely correlated with suppression of the fluctuations of the nanodot magnetic moments. Although the tunneling characteristics for the smallest nanodots can be described by Kondo physics, the possibility of observing Kondo phenomenon involving quantum dots with large magnetic moments requires a stronger theoretical foundation and remains an open question.

Acknowledgment. We thank Teya Topuria and Phil Rice for TEM data and analysis. We gratefully acknowledge useful discussions with Professors Sadamichi Maekawa, Jan Martinek, and David Goldhaber-Gordon.

Supporting Information Available: Sample preparation and measurement; definition of the Coulomb blockade temperature; estimate of the nanodot size and shape; superparamagnetic behavior of nanodots; influence of nanodot magnetic orientation on the TMR suppression. This material is available free of charge via the Internet at http://pubs.acs.org.

References

(1) Tsymbal, E. Y.; Mryasov, O. N.; LeClair, P. R. *J. Phys.: Condens. Matter* **2003**, *15*, R109.
(2) Parkin, S. S. P.; Kaiser, C.; Panchula, A.; Rice, P.; Hughes, B.; Samant, M.; Yang, S.-H. *Nat. Mater.* **2004**, *3*, 862−867.
(3) Yuasa, S.; Nagahama, T.; Fukushima, A.; Suzuki, Y.; Ando, K. *Nat. Mater.* **2004**, *3*, 868−871.
(4) Lee, Y. M.; Hayakawa, J.; Ikeda, S.; Matsukura, F.; Ohno, H. *Appl. Phys. Lett.* **2006**, *89* (4), 042506−3.
(5) Marukame, T.; Ishikawa, T.; Hakamata, S.; Matsuda, K.-i.; Uemura, T.; Yamamoto, M. *Appl. Phys. Lett.* **2007**, *90* (1), 012508−3.
(6) Butler, W. H.; Zhang, X.-G.; Schulthess, T. C.; MacLaren, J. M. *Phys. Rev. B* **2001**, *63*, 054416.
(7) Mitani, S.; Takahashi, S.; Takanashi, K.; Yakushiji, K.; Maekawa, S.; Fujimori, H. *Phys. Rev. Lett.* **1998**, *81*, 2799.
(8) Milner, A.; Gerber, A.; Groisman, B.; Karpovsky, M.; Gladkikh, A. *Phys. Rev. Lett.* **1996**, *76* (3), 475.
(9) Takahashi, S.; Maekawa, S. *Phys. Rev. Lett.* **1998**, *80* (8), 1758−1761.
(10) Sukegawa, H.; Nakamura, S.; Hirohata, A.; Tezuka, N.; Inomata, K. *Phys. Rev. Lett.* **2005**, *94* (6), 068304.
(11) Pustilnik, M.; Glazman, L. I. *J. Phys.: Condens. Matter* **2004**, *16*, R513−R537.
(12) Schelp, L. F.; Fert, A.; Fettar, F.; Holody, P.; Lee, S. F.; Maurice, J. L.; Petroff, F.; Vaurès, A. *Phys. Rev. B* **1997**, *56*, R5747−R5750.
(13) Yakushiji, K.; Ernult, F.; Imamura, H.; Yamane, K.; Mitani, S.; Takanashi, K.; Takahashi, S.; Maekawa, S.; Fujimori, H. *Nat. Mater.* **2005**, *4*, 57−61.
(14) Fettar, F.; Lee, S.-F.; Petroff, F.; Vaures, A.; Holody, P.; Schelp, L. F.; Fert, A. *Phys. Rev. B* **2002**, *65*, 174415.
(15) Ernult, F.; Yamane, K.; Mitani, S.; Yakushiji, K.; Takanashi, K.; Takahashi, Y. K.; Hono, K. *Appl. Phys. Lett.* **2004**, *84* (16), 3106−3108.
(16) Zeller, H. R.; Giaver, I. *Phys. Rev.* **1969**, *181* (2), 789.
(17) Gittleman, J. I.; Abeles, B.; Bozowski, S. *Phys. Rev. B* **1974**, *9*, 3891−3897.
(18) Yakushiji, K.; Mitani, S.; Takanashi, K.; Ha, J.-G.; Fujimori, H. *J. Magn. Magn. Mater.* **2000**, *212*, 75−81.
(19) Martinek, J.; Utsumi, Y.; Imamura, H.; Barnas, J.; Maekawa, S.; Konig, J.; Schön, G. *Phys. Rev. Lett.* **2003**, *91* (12), 127203.
(20) López, R.; Sánchez, D. *Phys. Rev. Lett.* **2003**, *90*, 116602.
(21) Martinek, J.; Barnas, J.; Fert, A.; Maekawa, S.; Schön, G. *J. Appl. Phys.* **2003**, *93* (10), 8265−8270.
(22) Pasupathy, A. N.; Bialczak, R. C.; Martinek, J.; Grose, J. E.; Donev, L. A. K.; McEuen, P. L.; Ralph, D. C. *Science* **2004**, *306* (5693), 86−89.
(23) Kouwenhoven, L.; Glazman, L. *Physics World*, January, 2001, pp 33−38.
(24) Romeike, C.; Wegewijs, M. R.; Hofstetter, W.; Schoeller, H. *Phys. Rev. Lett.* **2006**, *96*, 196601.
(25) Romeike, C.; Wegewijs, M. R.; Hofstetter, W.; Schoeller, H. *Phys. Rev. Lett.* **2006**, *97*, 206601.
(26) Goldhaber-Gordon, D.; Shtrikman, H.; Mahalu, D.; Abusch-Magder, D.; Meirav, U.; Kastner, M. A. *Nature* **1998**, *391*, 156−159.
(27) Cronenwett, S. M.; Oosterkamp, T. H.; Kouwenhoven, L. P. *Science* **1998**, *281* (5376), 540−544.
(28) Bermon, S.; Paraskevopoulos, D. E.; Tedrow, P. M. *Phys. Rev. B* **1978**, *17*, 2110.
(29) Goldhaber-Gordon, D.; Göres, J.; Kastner, M. A.; Shtrikman, H.; Mahalu, D.; Meirav, U. *Phys. Rev. Lett.* **1998**, *81*, 5225−5228.
(30) Liang, W.; Shores, M. P.; Bockrath, M.; Long, J. R.; Park, H. *Nature* **2002**, *417*, 725.
(31) van der Wiel, W. G.; Franceschi, S. D.; Fujisawa, T.; Elzerman, J. M.; Tarucha, S.; Kouwenhoven, L. P. *Science* **2000**, *289* (5487), 2105−2108.
(32) Faure-Vincent, J.; Tiusan, C.; Bellouard, C.; Popova, E.; Hehn, M.; Montaigne, F.; Schuhl, A. *Phys. Rev. Lett.* **2002**, *89*, 107206.
(33) Katayama, T.; Yuasa, S.; Velev, J.; Zhuravlev, M. Y.; Jaswal, S. S.; Tsymbal, E. Y. *Appl. Phys. Lett.* **2006**, *89* (11), 112503−3.
(34) Glazman, L. I.; Pustilnik, M., Coulomb blockade and Kondo effect in quantum dots. In *New Directions in Mesoscopic Physics (Towards Nanoscience)*; Fazio, R., Gantmakher, V. F., Imry, Y., eds.; Kluwer: Dordrecht, 2003; pp 93−115.
(35) Gould, C.; Slobodskyy, A.; Supp, D.; Slobodskyy, T.; Grabs, P.; Hawrylak, P.; Qu, F.; Schmidt, G.; Molenkamp, L. W. *Phys. Rev. Lett.* **2006**, *97* (1), 017202−4.
(36) Parks, J. J.; Champagne, A. R.; Hutchison, G. R.; Flores-Torres, S.; Abruna, H. D.; Ralph, D. C. *Phys. Rev. Lett.* **2007**, *99*, 026601.

NL072930N